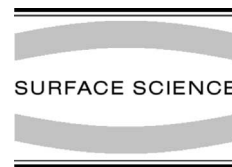




ELSEVIER

Surface Science 493 (2001) 460–474



www.elsevier.com/locate/susc

Terrace-width distributions and step–step repulsions on vicinal surfaces: symmetries, scaling, simplifications, subtleties, and Schrödinger

T.L. Einstein ^{a,*}, Howard L. Richards ^b, Saul D. Cohen ^a, O. Pierre-Louis ^c

^a Department of Physics, University of Maryland, College Park, MD 20742-4111, USA

^b Department of Physics, Texas A&M University – Commerce, Commerce, TX 75429, USA

^c LPS Grephe, UJF (CNRS) Grenoble I, B.P. 87, 38402 St Martin d'Hères, France

Received 17 October 2000; accepted for publication 7 December 2000

Abstract

For more than three decades, measurement of terrace width distributions (TWDs) of vicinal crystal surfaces have been recognized as arguably the best way to determine the dimensionless strength \tilde{A} of the elastic repulsion between steps. For sufficiently strong repulsions, the TWD is expected to be Gaussian, with \tilde{A} varying inversely with the squared variance. However, there has been a controversy over the proportionality constant. From another perspective the TWD can be described as a continuous generalized Wigner distribution (CGWD) essentially no more complicated than a Gaussian but a much better approximation at the few calibration points where exact solutions exist. This paper combines concisely the experimentally most useful results from several earlier papers on this subject and describes some advancements that are in progress regarding numerical tests and in using Schrödinger-equation formalism to give greater understanding of the origin of the CGWD and to give hope of extensions to more general interaction potentials between steps. There are many implications for future experiments. © 2001 Elsevier Science B.V. All rights reserved.

Keywords: Equilibrium thermodynamics and statistical mechanics; Stepped single crystal surfaces; Surface structure, morphology, roughness, and topography; Surface energy; Vicinal single crystal surfaces

1. Introduction

Quantitative measurement of the widths ℓ of terraces on vicinal surfaces became possible a decade ago. A principal motivation for examining the terrace width distribution (TWD) is the reco-

gnition that it provides arguably the optimal way to assess the strength of the elastic (and/or dipolar) repulsion between steps, specifically the coefficient A of the elastic repulsion per length A/ℓ^2 . Here the elastic repulsion is taken to be perpendicular to the mean step direction. All standard analysis procedures make a continuum approximation in the direction along the steps, called \hat{y} in “Maryland notation.” (The perpendicular direction in the terrace plane, in the “downstairs” direction, is denoted \hat{x} .) Hereafter, A appears only in form of a *dimensionless interaction strength*

* Corresponding author. Tel.: +1-301-405-6147; fax: +1-301-314-9465.

E-mail address: einstein@physics.umd.edu (T.L. Einstein).

$$\tilde{A} \equiv A\tilde{\beta}(k_{\text{B}}T)^{-2}, \quad (1)$$

where $\tilde{\beta}$ is the step stiffness.

Experimentally, a TWD is typically characterized by its variance σ^2 and, at least when \tilde{A} is not small, has a shape that can be satisfactorily approximated by a Gaussian. The Gaussian form can be readily derived from a mean-field (Gruber–Mullin (GM)) [1,2] argument, which produces an expression relating the variance to \tilde{A} . In recent years, theories from two new viewpoints have deduced different relations of \tilde{A} to the variance of the Gaussian. More recently, we have recognized that the TWD might better be described using a simple expression arising from random matrix theory, called the “generalized Wigner surmise.” As these results emerged, they have been published in several different articles [3–6]. The goal of the present paper is to collect succinctly the important results, to provide a global view of progress on this problem, to preview forthcoming results [7], and to point out areas where further progress is needed.

The following initial comments indicate our guiding philosophy: (1) The continuum approximation noted above is part of the step continuum approach to vicinal surfaces. In this perspective [8], the mesoscopic behavior of the step is characterized in terms of three parameters: the step stiffness $\tilde{\beta}$, the interaction strength A (or its equivalent), and a parameter representing the dominant kinetics (a kinetic coefficient or diffusion constant times carrier density). Hence, a knowledge of \tilde{A} is crucial to a proper description. (2) In this approximation, because step overhangs are physically forbidden, the set of step configurations in 2-D space maps into the world lines describing the evolution of non-crossing particles (spinless fermions or hard bosons) in 1-D space. This mapping is what leads to most of the progress in theoretical understanding. (3) In experiments to date, investigators have measured the distribution of terrace widths ℓ . This correlation function in essence is a many-particle correlation function, since one measures the probability of finding a pair particles separated by ℓ with none between them. (It is much easier for theorists to compute the probability of finding a pair particles separated by ℓ , regardless of how many particles are between them; note that

this two-particle correlation function should be equivalent to the many-particle function for step separations much smaller than the mean separation $\langle \ell \rangle$.)

In experimental systems (cf. Table 2, below), \tilde{A} is typically between 0 and 15 [4,5,8]. (While occasional values up to nearly 4000 have been reported [9] for \tilde{A} , our belief is that values above about 20–25 are indicative of anomalous behavior of some sort.) Exact theoretical information is available only for $\tilde{A} = 0$ and $\tilde{A} = 2$ [10,11], as well as in the limit $\tilde{A} \rightarrow \infty$ [12–14]. Hence, to assess the merits of various approaches for general \tilde{A} , we have generated well-characterized distributions numerically. We have then compared each of the theoretical predictions with these calibration standards.

In Section 2 we collect and synthesize the main results first for the traditional Gaussian analysis of TWDs and the competing ways of interpreting their variance in terms of \tilde{A} , then for the generalized Wigner distribution arising from the theory of fluctuating systems. Section 3 recounts concisely several highlights of previous explorations of these ideas. These include useful results on fitting procedures, an estimate of when discreteness becomes important, and a procedure to gauge how many independent measurements are contained in an image. Section 4 gives a brief summary of findings in applications to experimental data, with an emphasis on trends. In Section 5 we present previews of unpublished results concerning new directions in understanding TWDs with greater insight and in more complicated situations. Finally we offer brief conclusions and comments on connections with other active subjects in condensed matter physics.

2. Key results

2.1. Gaussian approximations to terrace width distributions

It is convenient and natural to divide ℓ by its average value, thus constructing the dimensionless parameter $s \equiv \ell/\langle \ell \rangle$. Then the TWD, $P(s)$, is not just normalized but has unit mean. The Gaussian approximation to the TWD is then written:

$$P(s) \approx P_G(s) \equiv \frac{1}{\sigma_G \sqrt{2\pi}} \exp \left[-\frac{(s-1)^2}{2\sigma_G^2} \right]. \quad (2)$$

Gaussians are typically chosen, not just for their simplicity, but because their use can be justified readily for strong elastic repulsion between steps. In this limit the motion of each step tends to be confined near its mean position, a GM argument (in which a single step is treated as active and its two neighbors are fixed at twice $\langle \ell \rangle$) shows that [1,2]

$$\sigma^2 = K_X \tilde{A}^{-1/2}, \quad (3)$$

where the subscript X anticipates that there will be different proportionality constants in different approximation schemes, indicated by X. For the GM case, with interactions only between nearest-neighbor steps, $K_{GM(NN)} = 1/\sqrt{48} \approx 0.144$. For the GM case, if all steps are allowed to interact with A/ℓ^2 , then 48 in $K_{GM(NN)}$ is replaced by $8\pi^4/15 \approx 52$, decreasing the variance by a scant 3⁺%; i.e., $K_{GM(all)} \approx 0.139$.

The Grenoble group [15,16] pointed out recently that the variance in Eq. (3) using K_{GM} underestimates (for given \tilde{A}) the true variance. Their arguments are based on two ideas. First, the contribution of the entropic repulsion decreases with increasing energetic repulsion; physically, large energetic repulsions diminish the chance of neighboring steps approaching each other, where the non-crossing condition underlying the entropic repulsion becomes significant. Thus, for very large \tilde{A} the entropy of interaction becomes negligible, so that the only entropy is that of the individual steps. Secondly, if both steps bounding a terrace fluctuate independently, then the variance of the TWD should be the *sum* of the variances of the fluctuations of each step, i.e. *twice* the variance obtained in the GM picture (in which there is a *single* “active” step between a pair of straight/rigid neighboring steps). This factor is reduced modestly by corrections due to the (anti)correlations [17] of neighboring steps. As a result, in this perspective the factor of 48 in $K_{GM(NN)}$ should decrease to 14.80, increasing the variance for a particular \tilde{A} by a factor of 1.801.

Including entropic repulsions in an average way (mnemonically denoted X = EA, the two underlined letters) [3] rather than discarding them extends to smaller \tilde{A} the range of viability of this (modified) asymptotic limit. Explicitly, \tilde{A} is replaced in Eq. (3) by an effective interaction strength \tilde{A}_{eff} obtained from the cubic term of the expansion of the projected free-energy of a vicinal surface as a function of misorientation slope [18]. The resulting enhancement is

$$\begin{aligned} \frac{\tilde{A}_{\text{eff}}}{\tilde{A}} &\equiv \frac{1}{4\tilde{A}} \left(\sqrt{4\tilde{A} + 1} + 1 \right)^2 \\ &\sim 1 + \tilde{A}^{-1/2} + \frac{\tilde{A}^{-1}}{2} + \dots \end{aligned} \quad (4)$$

Explicitly, Eq. (3) becomes $\sigma^2 \sim K_{EA} \tilde{A}_{\text{eff}}^{-1/2}$, with values for K_{EA} given in Table 1. In this case, $K_{EA(NN)}$ is nearly 10% larger than $K_{EA(all)}$.¹ Since this approach represents the limit of minimally important entropic interactions, presumably this large ratio is an upper bound, approached for large \tilde{A} , while the smaller (3⁺%) ratio of the GM case is more appropriate for weaker \tilde{A} . (In the free-fermion limit ($A = 0$), the NN and “all” cases obviously must be the same!)

The preceding approaches make a continuum approximation along the “time-like” \hat{y} -direction but maintain discrete steps. By making a continuum approximation in the x -direction as well and invoking correlation functions from roughening theory (so denoted X = R), the Saclay group [17,21,22] arrived at a result of the form of Eq. (3), again with \tilde{A}_{eff} replacing \tilde{A} , in which $K_R = 2/\pi^2 \approx 0.203$.

Since the various Gaussian approaches make different fundamental approximations, the detailed relationships between the width of the Gaussian and \tilde{A} differ notably. Even when a TWD can be well fit by a Gaussian, the estimation of \tilde{A} can be ambiguous.

¹ A value equivalent to $K_{EA(all)} = 0.247$ was found explicitly in a calculation using the harmonic, lattice approximation of the Calogero–Sutherland model [14], as well as implicitly in earlier studies [12,19,20], and seems to be the exact asymptotic coefficient [13].

Table 1
 Tabulation of predictions of the variance of terrace-width distributions $P(s)$ (where s is the terrace width normalized by its average value) based on exact results at the three soluble values of the dimensionless interaction strength, \tilde{A} , the corresponding Wigner-surmise expression, and several ways of interpreting a Gaussian fit

Property	Case	Abbrev.	Reference	$q = 2$ Non-interact	$q = 4$ Exact rpl.	Arbitrary q Repulsive	$q \rightarrow \infty$ Extreme rpl.
$q = 1 + \sqrt{1 + 4\tilde{A}} \equiv 2\sqrt{\tilde{A}_{\text{eff}}}$		X		$\tilde{A} = 0$	$\tilde{A} = 2$	$\tilde{A} = (q - 2)q/4$	$\tilde{A} \rightarrow \tilde{A}_{\text{eff}} \equiv q^2/4$
Symmetry assoc. w/Sutherland \mathcal{H}				Unitary	Symplectic		[SHO + phonons]
$a_q = 2[\Gamma(\frac{q+2}{2})]^{q+1} / [\Gamma(\frac{q+1}{2})]^{q+2}$			[10,11]	$32/\pi^2$	$(64/9\pi)^3$	In leftmost	$2 \exp[(q+3)/2]$
$b_q = [\Gamma(\frac{q+2}{2}) / \Gamma(\frac{q+1}{2})]^2$				$4/\pi$	$64/9\pi$	column	$q/2 + 1/4$
Variance $\sigma^2 = \mu_2 = \mu_2 - 1$	Exact Wigner surmise	[all] W [all]	[10,11] [3,10,27]	0.180 0.1781	0.105 0.1045	$(q+1)/2b_q - 1$	$0.495/q$ $0.500/q$
Gaussian alternatives	<i>Gruber–Mullins</i> ,, <i>Modified Grenoble</i> ,, <i>Saclay</i>	GM(all) GM(NN) EA(all) EA(NN) R [all]	[1] ,, [3,15,16] ,, [17,21,22]	0.1307 0.1307 – – 0.203	0.0981 0.1021 0.1185 0.1300 0.101	$0.139/\sqrt{\tilde{A}}$ $0.144/\sqrt{\tilde{A}}$ $0.247/\sqrt{\tilde{A}_{\text{eff}}}$ $0.260/\sqrt{\tilde{A}_{\text{eff}}}$ $0.203/\sqrt{\tilde{A}_{\text{eff}}}$	$0.278/q$ $0.289/q$ $0.495/q$ $0.520/q$ $0.405/q$
Neighboring terraces	Exact $\langle (s_1 + s_2 - 2)^2 \rangle$ Multistep CGWD		[10] [42]	0.248 0.257	0.138 0.145		0^+ 0^+

The “unmodified” Grenoble expression [15,16] is obtained by substituting \tilde{A} for \tilde{A}_{eff} . The entries for the variance at $\tilde{A} = 2$ are almost 50% larger. The bracketed “[all]” is a reminder that the Calogero–Sutherland model – and, hence, the exact solutions and the Wigner surmises – involves all steps interacting. As \tilde{A} increases, the TWD becomes narrower, more symmetric, and more nearly Gaussian. Anticorrelations of neighboring terrace-width fluctuations increase. For the three exactly-solvable [non-trivial] cases, the Wigner surmise provides an excellent approximation, significantly better than any alternative.

The covariance of the fluctuations of neighboring steps is the difference from unity of the tabulated correlation $\langle (s_1 + s_2 - 2)^2 \rangle$ divided by twice the variance. It is negative, indicating that fluctuations of adjacent terrace widths are anticorrelated. For GM this covariance is *ipso facto* – 1. With the Grenoble formalism [15,16] we find it to be $-1/3$ (NN) or $-0.36 \dots$ (all); with the Saclay formalism [21], it is -0.33 . In all these cases, the covariance is independent of \tilde{A} . In contrast, the exact covariance is independent of \tilde{A} . In contrast, the exact covariance increases weakly in magnitude with \tilde{A} , from -0.31 at $\tilde{A} = 0$ to -0.34 at $\tilde{A} = 2$ [10], and presumably to -0.36 asymptotically.

2.2. Symmetry and Wigner approximation to terrace width distributions: continuous generalized Wigner distribution

In considering high-lying energy levels in nuclei, Wigner long ago proposed that fluctuations in their spacings in energy should exhibit certain universal features depending only on the symmetry – orthogonal, unitary, or symplectic – of the couplings. This work, embedded in random-matrix theory [10,11], has had profound and widespread implications for characterizing a wide range of fluctuation phenomena [11,14] in chaotic systems, since TWDs are an example of equilibrium fluctuations [3–5]. The explicit connection to this body of knowledge is based on the description of steps using the (Calogero [23,24]) Sutherland [25,26] model of spinless fermions on a large ring (essentially 1-D with periodic boundary conditions) interacting with a repulsion decaying as the inverse square of separation. Remarkably, the distribution of interparticle spacings along the ring (i.e. the TWD) is equivalent to the distribution of the above-mentioned energy spacings, which can be solved exactly by random-matrix methods for the three symmetries. According to the so-called Wigner surmise, these three exact solutions for the distribution of fluctuations can be approximated by [3]

$$P_\varrho(s) = a_\varrho s^\varrho \exp(-b_\varrho s^2). \tag{5}$$

The three symmetries correspond to the values $\varrho = 1, 2,$ or $4,$ respectively. The constants b_ϱ (associated with unit mean of $P(s)$) and a_ϱ (deriving from normalization) are

$$b_\varrho = \left[\frac{\Gamma(\frac{\varrho+2}{2})}{\Gamma(\frac{\varrho+1}{2})} \right]^2 \quad \text{and} \quad a_\varrho = \frac{2b_\varrho^{(\varrho+1)/2}}{\Gamma(\frac{\varrho+1}{2})}. \tag{6}$$

This surmise was used to describe the spacings not of particles in real space but rather of energy levels, first in nuclei, later in chaotic systems [27] (Fig. 1).

The variance of $P_\varrho(s)$ is just

$$\sigma_w^2 = \frac{\varrho + 1}{2b_\varrho} - 1 \underset{\varrho \rightarrow \infty}{\sim} \frac{1}{2\varrho}. \tag{7}$$

The three symmetries correspond to the values $\varrho = 1, 2,$ or $4,$ respectively. The approximations

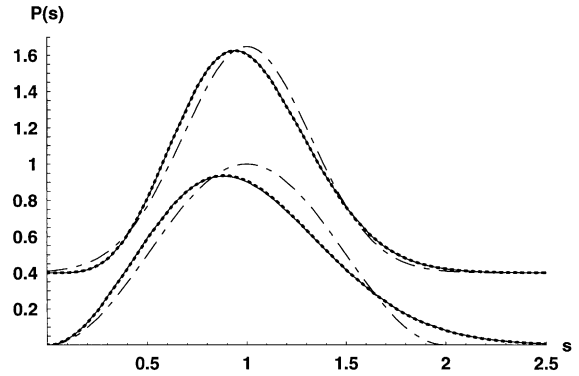


Fig. 1. $P(s)$ vs. $s \equiv \ell/\langle \ell \rangle$ for the [sixth approximant [38] to the exact “free fermion”, $\tilde{A} = 0$ result (solid curve), the GM approximation $\sin^2(\pi s/2)$ (long-short dashed curve), and the $\varrho = 2$ Wigner surmise result (dotted curve), barely distinguishable from the exact result). Offset upward by 0.4 for clarity, a similar plot of an approximant of the exact result for $\tilde{A} = 2$ [38], the GM Gaussian approximation $(24/\pi^2)^{1/4} \exp(-\sqrt{24}(s - 1)^2)$ (long-short dashed curve), and the $\varrho = 4$ Wigner surmise result (dotted curve).

prove to be outstanding, accurate to better than ± 0.004 for the latter two cases (cf., esp., Fig. 4.2a of Ref. [27]). From the mapping of the step problem onto the Sutherland Hamiltonian [24,25] comes the relation

$$\tilde{A} = \varrho(\varrho - 2)/4. \tag{8}$$

(By inverting Eq. (8) to obtain ϱ as a function of \tilde{A} , we can make the important and useful identification of ϱ as $2\sqrt{\tilde{A}_{\text{eff}}}$, as given in Eq. (4).)

For the three special values of ϱ , Eq. (5) accounts for the cases $\tilde{A} = -1/4, 0,$ or $2,$ respectively. The value 0 corresponds to steps interacting only via the entropic repulsion, whereas the negative value corresponds to an attraction, which cannot be produced by the generic elastic interaction between steps (except perhaps in abnormal cases in which there are strong in-plane dipoles at the step edges [18,28]). The third case, $\tilde{A} = 2,$ corresponds to a rather moderate repulsion. As documented in Table 1, the variance of Wigner’s $P_\varrho(s)$ is nearly the same as the exact value. The Sclay and the GM estimates are a few percent too low, while the modified Grenoble estimate is much too high.

The crucial question is what to do for more general values of \tilde{A} . We simply use Eq. (5) for arbitrary value of $\varrho \geq 2$, with ϱ related to \tilde{A} by Eq. (8). For brevity, we refer hereafter to this distribution, for general ϱ , as the continuum generalized Wigner distribution (CGWD). In contrast to the three special cases, there are no symmetry arguments to justify the CGWD form. We offer the following arguments in its support, although ultimately one must rely on numerical checks.

(1) It seems plausible that $P_\varrho(s)$ is a decent approximation of the TWD for values of ϱ between 2 and 4 since the range in parameter space is small. In any case, the arguments supporting the approaches leading to any of the Gaussian approximations fail in this regime.

(2) Extrapolation of the CGWD to values of ϱ greater – possibly much greater – than 4 is of more concern. For very large \tilde{A} , the argument underlying the Grenoble viewpoint becomes compelling. In this limit, the leading term in the expansion of σ_W^2 in Eq. (7) implies that $K_W = 1/4$ in Eq. (3), with \tilde{A}_{eff} replacing \tilde{A} . Thus, as listed in Table 1, the CGWD variance approaches the (modified) Grenoble estimate nicely, while the Saclay estimate is notably too small. Since the CGWD does well in the limit of very large ϱ as well as at $\varrho = 4$, it is a promising candidate for an interpolation method between these values.

(3) As a function of s , the CGWD not only has the Gaussian behavior expected (based on analogies with random walkers) at large step separations but also reproduces the exact power of s for $s \ll 1$: In this limit, the many-step correlation function becomes identical to the pair correlation function, due to the vanishing probability of any other step lying between the pair of steps separated by s . Several workers have shown that in this limit, the pair correlation function is proportional to s^ϱ , with a prefactor similar (within at least a few percent for physical values of ϱ) to a_ϱ [12,20,29–31].

(4) We can derive the CGWD from a Schrödinger-equation approach [6], as discussed below in Section 5.2. This approach has the further benefit of allowing one to consider more general potentials than the asymptotic form of the elastic repulsion.

2.3. Preliminary numerical results

To test numerically the accuracy of Eq. (5) we apply standard Monte Carlo methods to the most elementary model that contains the necessary physics, the terrace–step–kink (TSK) model. In the TSK model the only thermal excitations are kinks of energy ϵ along the steps. The stiffness $\tilde{\beta}_{\text{TSK}}$ of an isolated step – needed to extract A from \tilde{A} – is simply $2k_B T (a_\parallel/a_\perp^2) \sinh^2(\epsilon/2k_B T)$ [32]. Here a_\parallel is the unit spacing along a step edge (\hat{y}), and a_\perp is the \hat{x} component of a kink. This model is obviously *discrete* in the \hat{y} as well as the \hat{x} -directions [2,17,22,32]. For simplicity we consider a vicinal simple-cubic lattice with unit lattice constant. Periodic boundary conditions are imposed in both directions. To minimize finite-size effects, the length of the system in the \hat{y} -direction, L_y , should be substantially larger than the characteristic distance y_{coll} along \hat{y} between close approaches of adjacent steps: $\langle \ell \rangle^2 \tilde{\beta}/k_B T$ [32]. The choice of the mean spacing between steps requires particular care. We shall show below that if $\langle \ell \rangle$ is 4 or smaller, finite size effects may contaminate the results extracted from the CGWD (since it is based on a continuum approximation). On the other hand the minimum acceptable value of L_y increases like $\langle \ell \rangle^2$. Furthermore, too low a temperature results in slow dynamics and a high stiffness, making demands on L_y , while too high a temperature leads excessive step wandering and breakdown of the approximations underlying the viability of the TSK model. We are preparing a careful discussion of these considerations [7], which includes transfer-matrix calculations in addition to Monte Carlo simulations.

In Fig. 2 we provide some preliminary results for the case $\langle \ell \rangle = 6$ at $k_B T/\epsilon = 0.5$, with $L_y = 200$ and the number of steps $N = 10$. In addition to the standard Metropolis algorithm [33], we use the “refusal-free” n -fold way [34,35], especially for large \tilde{A} (or at low T). There it is much more efficient than the Metropolis algorithm, which requires many attempts before making a change. The elastic repulsion is here considered only between neighboring steps, a common simplification in Monte Carlo [2,21], with the accordant modest underestimate of σ^2 noted in subsection 2.1. (In Ref. [7] we will also extend the inverse-square

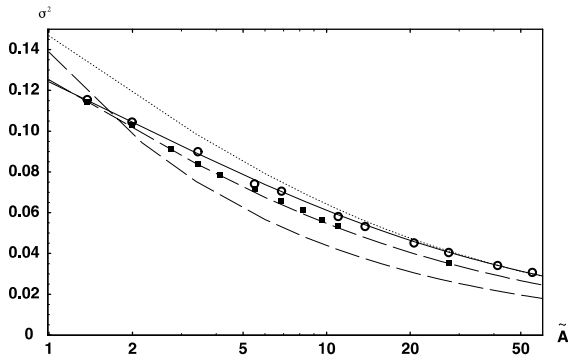


Fig. 2. Plot of the variance σ^2 as a function of \tilde{A} on a logarithmic scale. Plotted for the CGWD [“Wigner distribution”] (solid curve), the modified Grenoble (dotted curve) and Saclay (long dashed curve) Gaussian distributions, and the GM Gaussian approximation (long-short dashed curve). The CGWD curve passes essentially directly over the exact value of the variance at $\tilde{A} = 2$. Monte Carlo data generated using the Metropolis algorithm are depicted by ■’s; data produced with the n -fold way algorithm are shown as ○’s.

repulsions to further neighbors.) Our algorithm includes “corner exclusion” in addition to standard edge exclusion, based on some evidence that it provides the better discrete analogue of the continuum model; the consequent modest upward shift of σ^2 is in the opposite direction of that due to restriction to nearest-neighbor step-step repulsions (see Ref. [7] for more details.).

Along with the numerical results, the various predictions of the variance are plotted as functions of the physical variable \tilde{A} . A logarithmic scale is used for the horizontal axis so as not to give undue visual emphasis to larger values of \tilde{A} nor to blur the region of rapid variation for small \tilde{A} , for which an exact calibration point exists. The physical values of \tilde{A} range from near 0 up to the mid teens. A few larger values have been reported [9], but there are suspicions that more than simple elastic repulsions are involved. There are relatively few reports of small but non-zero values of \tilde{A} . We suspect that one reason is that any of the Gaussian approximations manifestly fail in this regime because the distribution becomes strongly skewed.²

² However, the idea of estimating \tilde{A} using this skewness [3] did not prove to be fruitful when confronting experimental data [4].

Before the recognition of the utility of the Wigner distribution, one could not deal quantitatively with small \tilde{A} [36].

3. Useful results for interpreting experiments

3.1. Extracting \tilde{A} from variance

If one accepts the CGWD as the optimal way to analyze TWDs, then Eq. (7) shows how to estimate the variance from \tilde{A} . However, experimentalists usually seek the reverse. An excellent estimate [5] of \tilde{A}_W from the variance can be derived by expanding σ_W^2 as given in Eq. (7) in powers of ϱ^{-1} . This series can then be reverted to give ϱ as a function of σ^2 [5]. Then using Eq. (8) gives the estimate

$$\tilde{A} \approx \frac{1}{16} \left[(\sigma^2)^{-2} - 7(\sigma^2)^{-1} + \frac{27}{4} + \frac{35}{6} \sigma^2 \right], \tag{9}$$

with all four terms needed to provide a good approximation over the full physical range of \tilde{A} . The Gaussian methods described earlier essentially use just the first term of this expression and adjust the prefactor. When \tilde{A} is not weak (see Ref. [5] for explicit guidelines.), those who for some reason prefer not to use Eq. (5) to gauge ϱ (and thence \tilde{A}) can extract the variance from a Gaussian fit and then applying Eq. (9) is a reasonable procedure.

When dealing with tabulations of data analyzed in the traditional way [8], i.e. using the inverse of Eq. (3) with $X = \text{GM}(\text{NN})$, it is useful to recast Eq. (9) in a form that indicates the factor by which the estimate \tilde{A}_W based on CGWD exceeds the traditional estimate $\tilde{A}_{\text{GM}(\text{NN})}$ (denoted \tilde{A}_G for brevity):

$$\tilde{A}_W / \tilde{A}_G \left[\equiv A_W / A_G \right] \approx 3 - 21\sigma^2 + \frac{81}{4}\sigma^4 + \frac{35}{2}\sigma^6. \tag{10}$$

As noted parenthetically, Eq. (1) implies that the ratio of the physical interaction strengths is the same as that of the dimensionless strengths. Since $A \propto \tilde{A}$ we can use this relation in Table 2 to update tabulated A ’s in Ref. [8] (based on GM).

Table 2
Compendium of experiments measuring the variances of terrace width distributions of vicinal systems

Vicinal	T (K)	σ^2	ϱ	\tilde{A}	A_W/A_G	A_W (eV Å)	Experimenters
Pt(110)-(1 × 2)	298		2.2	0.13	–	$\tilde{\beta} = ?$	Swamy, Bertel [36]
Cu(19, 17, 17)	353	0.122	4.1	2.2	0.77	0.005	Geisen [5,54]
Si(111)	1173	0.11	3.8	1.7	0.96	0.4	Bermond, Métois [55]
Cu(1,1,13)	348	0.091	4.8	3.0	1.27	0.007	Giesen [5,56]
Cu(11,7,7)	306	0.085	5.1	4	1.37	0.004	Geisen [5,54]
Cu(111)	313	0.084	5.0	3.6	1.39	0.004	Geisen [5,54]
Cu(111)	301	0.073	6.0	6.0	1.58	0.006	Geisen [5,54]
Ag(100)	300	0.073	6.4	6.9	1.58	$\tilde{\beta} = ?$	P. Wang. . .Williams
Cu(1, 1, 19)	320	0.070	6.7	7.9	1.64	0.012	Geisen [5,56]
Si(111)-(7 × 7)	1100	0.068	6.4	7.0	1.67	0.7	Williams [57]
Si(111)-(1 × 1)Br	853	0.068	6.4	7.0	1.67	0.1	X.-S. Wang, Williams [58]
Si(111)-Ga	823	0.068	6.6	7.6	1.67	1.8	Fujita. . .Ichikawa [59]
Si(111)-Al $\sqrt{3}$	1040	0.058	7.6	10.5	1.85	2.2	Schwenicke. . .Williams [60]
Cu(1, 1, 11)	300	0.053	8.7	15	1.95	0.02	Barbier et al. [21]
Cu(1, 1, 13)	285	0.044	10	20	2.12	0.02	Geisen [5,56]
Pt(111)	900	0.020	24	135	2.59	6	Hahn. . .Kern [61]
Si(113) rotated	1200	0.004	124	3.8×10^3	2.92	$(27 \pm 5) \times 10^2$	van Dijken, Zandvliet, Poel-sema [9]

The estimate of \tilde{A} is obtained from the (normalized) variance using Eq. (9), except for the first-row entry, which is based on a direct fit using the 2-parameter CGWD. A_G is short for $A_{GM(NN)}$, the conventional estimate (cf. Table 7 of Ref. [8]). The column “ A_W/A_G ”, computed using Eq. (10), shows that for most systems the correction factor is of order half the ultimate asymptotic factor. For the copper entries, A_W is computed from Eq. (1), using $\tilde{\beta}_{TSK} = 2k_B T(a_0/a_1^2) \sinh^2(\epsilon/2k_B T)$ and kink energies ϵ of 0.126 and 0.12 for vicinals to {100} [nominally (1, 1, 2n + 1)] and {111}, respectively. In other cases, A_W is simply rescaled from Ref. [8]. In two cases, the values of the stiffness are not readily available.

3.2. Gaussian fits of the generalized Wigner distribution

Since TWDs for strong repulsions are well described by Gaussians, one expects – and finds – that the CGWD should be well approximated by a Gaussian in this limit. In Ref. [5] a quantitative assessment is given of how closely the two distributions correspond as a function of ϱ . At the calibration point (for which an exact solution exists) for repulsive interactions ($\varrho = 4$), the relative difference of the standard deviation of a Gaussian fitted to $P_\varrho(s)$ from the actual standard deviation of this CGWD (viz. the square root of the second moment of $P_\varrho(s)$ about its mean of unity) is around 1%, and decreases monotonically with increasing ϱ . For this range ($\varrho \geq 4$) differences between estimates of \tilde{A} obtained from CGWD and the various Gaussian fit methods are predominantly due to different philosophies of extracting \tilde{A} from σ rather than from differences in the fitting methods.

In contrast to the Gaussian approximations, the peak of the CGWD must perforce (due to unit

mean) lie below one. Specifically, for $\tilde{A} = 0$ and 2, the maximum of $P_\varrho(s)$ occurs at $s = 0.886$ and 0.940, respectively, while the limiting value for strong repulsions is $1 - 0.125/\sqrt{\tilde{A}_{\text{eff}}}$ [3]. Formulas have been derived [5] indicating the errors in fitting ϱ due to errors in the first or zeroth moment of the distribution.

3.3. Wigner distribution as a two-parameter fit

In applications to experimental TWDs, the CGWDs giving the best fits sometimes have first moments that differ somewhat from the first moments of the data, especially in cases termed “poor data” [4,5] which exhibit a small “hump” at large values of s , beyond the peak near unity (see Section 4 below). Moreover, it can be desirable to determine the scaling length (the “effective mean,” which equals the first moment for ideal CGWDs) and the variance in a single fitting procedure rather than to predetermine this length from the first moment. This “refined” scaling implies that the argument of P_ϱ should be $\ell/\bar{\ell}$, where $\bar{\ell}$ denotes the

characteristic length determined along with ϱ in a two-parameter least-squares fit of the data to a CGWD. Since s is still determined from the raw data as $\ell/\langle\ell\rangle$, the refined scaling translates into replacing s by $s\langle\ell\rangle/\bar{\ell}$ in the argument of the distribution. If the integration variable s were similarly replaced, then the refined scaling would amount to a redefinition of a dummy variable, and normalization would still be realized. Since the independent variable is kept as s , we make the replacement:

$$P_{\varrho}(s) \rightarrow (\langle\ell\rangle/\bar{\ell})P_{\varrho}(s\langle\ell\rangle/\bar{\ell}) \quad \text{i.e.} \quad (\langle\ell\rangle/\bar{\ell})P_{\varrho}(\ell/\bar{\ell}). \quad (11)$$

In the specific applications to data in Sections 4.1 and 4.2, $\langle\ell\rangle/\bar{\ell}$ tends to be greater than unity, typically by several percent, but it is unclear whether this is true for semiconductors or other metals. In our companion Monte Carlo simulations [7], where we have greater control of purity and uniformity than in experiments, the optimal $\bar{\ell}$ is essentially identical to $\langle\ell\rangle$: there is no need for the added flexibility of the two-parameter fit.

3.4. Effects of lattice discreteness

For actual crystals as well as for the TSK model used in numerical simulations, the variable s cannot assume a continuum of values as implicitly assumed in writing Eqs. (5) and (6); the only possible values of ℓ are integer multiples of a_{\perp} , the interrow spacing in \hat{x} . If this restriction is placed on the values of ℓ used to generate the arguments s of Eq. (5), then we have constructed a *discrete* generalized Wigner distribution (DGWD).³ We use the same value of b_{ϱ} as in Eq. (6), even though it is no longer guaranteed to produce unit mean (or the same variance) as it does for the CGWD. Since these vicinals are technically rough, there is no need for $\langle\ell\rangle$ to be an integer multiple of a_{\perp} (or otherwise in registry with the terrace plane),

³ Discreteness also introduces the possibility of a roughening transition from a vicinal to a high-index-facet surface [22,37]. This interesting phenomenon does not seem to play a role in the physical systems under study here.

though it is common to make this choice in simulations.

Scaling of discrete TWDs for the free-fermion case ($\tilde{A} = 0$) was demonstrated nearly a decade ago [38]. Inspired thereby, we [5] explored the effects of discreteness, first choosing values of $\langle\ell\rangle$ and ϱ to specify a DGWD, then numerically performing two-parameter fits using CGWD formulae (Eqs. (5), (6) and (11)) to produce estimates of ϱ_c and (via Eq. (8)) \tilde{A}_c .

Among many minor observations, two major themes stand out: first, $\langle\ell\rangle \geq 4$, \tilde{A}_c provides a reasonable estimate of \tilde{A} over the range of physically reasonable dimensionless repulsions. Furthermore, at fixed values of \tilde{A} the error in \tilde{A}_c diminishes as $\langle\ell\rangle$ increases. Second, as the TWD becomes narrower (i.e. for sufficiently large \tilde{A} or ϱ), \tilde{A}_c becomes a questionable estimate for \tilde{A} ; study of the cases $\langle\ell\rangle/a_{\perp} = 2-6$ suggests that this breakdown occurs for ϱ near $(\langle\ell\rangle/a_{\perp})^2$. This threshold corresponds to the squared interstep spacing being comparable to the variance.

For very large \tilde{A} , seemingly just above the range of greatest physical significance, there are more general indications of the breaking down of the continuum approximation. For example, for \tilde{A} in the upper teens, there begin to be ambiguities in the application of Eq. (8) [7]. With periodic boundary conditions one can still get elementary excitations that are extended along a step (i.e. along \hat{y}), so long as they are “in phase” in \hat{x} , but with more realistic conditions (with various sorts of defects hindering the fluctuations of occasional steps), the elementary excitation becomes individual “teeth” (kink–antikink pairs separated by one spacing along \hat{y}) [39]. Then the idea of step stiffness also breaks down, and with it the concept of \tilde{A} (see Eq. (1)).

The main implication is that analyses of highly misoriented vicinal surfaces with CGWD should be viewed with caution. For example the (1 1 7) for close-packed steps on surfaces vicinal to {1 0 0} planes of fcc crystals corresponds to $\langle\ell\rangle = 3$. For {1 1 1} fcc surfaces, the corresponding Miller indices are (5 3 3) for A steps ({1 0 0} microfacets) and (2 2 1) for B steps ({1 1 1} microfacets) [40].

The obstacles posed by discreteness are not vagaries of Wigner distributions. High misorien-

tation causes similar problems when the mean and variance of discretized Gaussian TWDs are analyzed as though they were continuous Gaussian functions (see Ref. [5] for details).

3.5. Estimate of number of independent measurements

In order to estimate uncertainties in the determination of the TWD and, ultimately, \tilde{A} , it is important to have a realistic value of the number of *independent* measurements, a number generally much smaller than the total number of measurements. To make a rough estimate, one can compute the correlation function [41] of the terrace widths $\ell_n(y)$ between steps n and $n + 1$:

$$C_n(y) = \frac{\sum_{n'}^{N-n} \sum_{y'=1}^{L_y-y} \ell_{n'}(y') \ell_{n'+n}(y'+y)}{(N-n)(L_y-y)} - \langle \ell \rangle^2 \quad (12)$$

is calculated, where N is the number of terraces in the image. The correlation function along the steps decays exponentially as $C_0(y) \sim \exp(-y/\xi_y)$, where ξ_y is proportional to y_{coll} (cf. Eqs. (5), (12), and (26) of Ref. [32]), but can be measured directly. The correlation function between steps is more complicated. As noted in Table 1, $C_1(0)$ is negative [10]; $|C_n(0)|$ tends to decrease rapidly with increasing n . Setting c as a small cutoff ($c = 0.1$ is recommended [5]), we determine y_c , the smallest value of y for which $|C_0(y)| \leq c$ when $y \geq y_c$, and n_c , the smallest n so that $|C_n(0)| \leq c$ for all $n \geq n_c$. Then the number of “independent” terrace widths will be approximately $(L_y/y_c)(N/n_c)$ rather than $L_y N$, as might be naively guessed. A rough test calculation [5] shows that the reduction factor can be nearly two orders of magnitude, emphasizing the need for using several STM images to obtain decent statistics.

4. Applications to experimental terrace width distributions

In two papers [4,5], we made extensive applications of the ideas presented above to Giesen’s voluminous data on vicinal Cu {100} and {111}

surfaces, each at three different misorientations, and these six cases at various temperatures. In all, around 30 different cases were considered. In addition, our ideas were tested successfully on data for vicinal Pt(110), which has a small \tilde{A} and so is not amenable to the Gaussian approaches used heretofore. The purpose of this section is to summarize the tabulations and discussions in those papers.

4.1. Copper: moderately strong repulsions

The Cu TWDs can be sorted into three groups based on a visual assessment of their quality [4, 5]: A “good” TWD changes height essentially monotonically below the peak and again above it; there is minimal scatter in the data points. An “OK” TWD has more scatter, with small dips and peaks introduced by variations (within the limits of the general margin of error) of single data points. A “poor” TWD has a double-peak or hump at large s ; correspondingly, the position of the (main) peak occurs noticeably below $s = 1$, even when the peak is fairly narrow and the skewness minimal. The judgment that this data is “poor” is based both on the intuition of the *experimenter* and on the following argument: A second peak at large s would be characteristic of the onset of faceting; however, “poor” data tends to occur at high temperatures, whereas faceting should be more important at low temperatures.

The data fits exhibited several general trends. In almost all cases, the value of $\bar{\ell}$ derived from the two-parameter fit to a CGWD is smaller than $\langle \ell \rangle$ given by the mean of the TWD (and the opposite shift in the exceptional cases is very small); likewise, the directly measured values of the variance are almost always larger than the values obtained by any of the three fitted curves (cf. Section 7 of Ref. [5]). The value of ϱ is higher for the two-parameter CGWD fit than for the single-parameter version, and the associated value of σ^2 typically closer to that deduced from the Gaussian fit. For “good” data, $\bar{\ell}/\langle \ell \rangle$ differs from unity by a few percent, and the change in ϱ and σ^2 is negligible. For “poor” data, $\bar{\ell}/\langle \ell \rangle$ is at least twice as far below unity, and the two-parameter-fit curve is narrower than the single-parameter-fit curve. The tails or

humps in the experimental TWDs seem to be responsible for the systematic discrepancies in the fits, especially the smaller mean and smaller variance of the fits relative to the direct measurements.

A remarkable consistency check was obtained for Cu (1 1 13) [4]. For a dozen values of temperature, $(k_B T)^2 \tilde{A}$ was plotted against T . Since A is expected to be relatively insensitive to thermal change, Eq. (1) predicts that the plotted curve should decrease like the stiffness. To within error bars, such behavior is found, where the stiffness is computed using an independently determined kink energy.

4.2. Platinum: weak repulsions

On vicinal Pt(1 1 0) at room temperature, the terraces are (1×2) reconstructed, and the steps correspond to 3-unit “ (1×3) ” segments. Recent measurements show that the interaction between their steps is small [36], rendering Gaussian approximations invalid. Fits to the CGWD yield $\varrho = 2.06$ ($\tilde{A} = 0.0309$) or, when done in the two-parameter way, $\varrho = 2.24$ ($\tilde{A} = 0.134$) [5]; in the latter case, the optimal $\bar{\ell}/\langle \ell \rangle$ is 91% and the fit is notably better. The presence of a high- s bulge indicates this feature is not peculiar to the vicinal Cu systems of GE.

4.3. Other systems

Additionally, in Table 2 we list the variances measured for several different experimental systems, along with the value of \tilde{A} deduced from the CGWD distribution via Eq. (9). The primary goal of this table is to display general trends in physical systems rather than to provide a comprehensive account of experiments to date. As asserted earlier, values of \tilde{A} are generally below the mid-teens. On the other hand, A ranges over orders of magnitude. If one accepts that the CGWD provides a good accounting in general for \tilde{A} as a function of the measured variance, then the column labeled A_W/A_G shows that for most systems, the underestimate by using the Gruber–Mullins approximation is roughly half that in the asymptotic limit.

5. New directions

5.1. Multistep distributions

Experiments to date have focused exclusively on the TWDs, ignoring the possibility of extracting the distributions of the distances between pairs of steps having n steps, $n = 1, 2$, or more, between them. This supplementary data could provide a valuable consistency check. For the three special cases $\varrho = 1, 2, 4$, these distributions have recently been investigated theoretically in a different context [42]. If in Eq. (5) we make the redefinition $s \equiv (\ell_1 + \dots + \ell_{n+1})/\langle \ell \rangle$ (ℓ being the terrace width), then this CGWD expression gives a good approximation of the multistep distribution, provided that the power-law exponent ϱ is replaced by

$$\varrho_n = n + \frac{(n+1)(n+2)}{2} \varrho, \quad (13)$$

where ϱ (or, equivalently, ϱ_0) is the exponent for the [single] TWD. The new constant b_{ϱ_n} is determined by the condition that the first moment of $P_{\varrho}(n, s)$ is $n+1$; besides replacing ϱ by ϱ_n in the Γ -function arguments in Eq. (6), a factor of $n+1$ must be included in the denominator. The normalization constant a_{ϱ_n} can be obtained simply by using b_{ϱ_n} and ϱ_n in the expression for a_{ϱ} in Eq. (6). As for TWDs, these results can be taken to apply to general values of ϱ .

Preliminary checks using Monte Carlo simulations of the TSK model, described above, find fine agreement with this multistep CGWD for the double-terrace-width ($n = 1$) case, but just adequate agreement for the case $n = 2$. Moreover, Table 1 shows that the variance of the sum over the widths of two adjacent terraces predicted by $P_{\varrho}(1, s)$ does not display the spectacular agreement with exact results seen for simple TWDs, viz. $n = 0$. We suspect that the agreement will further degrade as more widths are included (higher n 's considered), due to weakness in the main assumption in the derivation of Eq. (12): that the conditional probability density of occurrence of a step at a given distance from a fixed step, with n steps in between, can be expressed in terms of the $(n+1)$ th power of the corresponding probability for this distance with no intermediate steps.

5.2. Continuous generalized Wigner distribution and beyond via Schrödinger equations

As presented, the CGWD is formally justified only for the three special values of ϱ . Accordingly, we have developed arguments using Schrödinger equations to show that it can be expected to have the more general validity assumed above [6]. The formalism also allows treatment of more general potentials than the inverse-square term characterizing the long-range behavior of elastic interactions. Of particular physical importance are the higher-order terms that enter at smaller terrace widths and an oscillatory interaction mediated by electronic surface states.

We begin by defining a wave function $\psi_0(s)$ such that $\psi_0^2(s) \equiv P_\varrho(s)$. Differentiating twice and using Eq. (8), we find

$$-\frac{d^2}{ds^2}\psi_0(s) + \left[\tilde{A}s^{-2} - b_\varrho(\varrho + 1) + b_\varrho^2s^2\right]\psi_0(s) = 0. \quad (14)$$

The term $\tilde{V}(s) = \tilde{A}s^{-2}$ is the dimensionless step interaction. The term $\tilde{U}(s) = b_\varrho^2s^2$ is a dimensionless projected free energy representing interactions with all the other steps not explicitly considered. Clearly Eq. (14) can be understood as a Schrödinger equation, with $\psi_0(s)$ the (real) ground state wave function and with $b_\varrho(\varrho + 1)$. (To consider perturbations from pure inverse square interactions, one can generate all the eigenfunctions $\psi_n(s)$ of Eq. (14), which can be expressed as special functions (see Ref. [6] for details.) In this framework, by substituting more general potentials for $\tilde{A}s^{-2}$ in Eq. (14) and solving for the ground-state wavefunction, we can contend analytically with more complicated potentials. Successful tests are described in Ref. [6].

It is tantalizing to invert the preceding approach to deduce the underlying interaction potential from the experimental TWD. Since naive implementations prove to be dangerous, the recommended procedure [6] requires considerable computation: Initially, a parametric approximant of the unknown potential should be constructed using all available information; crude initial estimates must be made of the values of the parameters. If the tail of the experimental TWD is

Gaussian, a monotonically decaying $\tilde{V}(s)$ and a quadratic $\tilde{U}(s)$ are anticipated. (If the tail is exponential, $\tilde{U}(s)$ is linear in s , and $\tilde{V}(s)$ can be nonmonotonic.) Then the choice of parameters is optimized by iteratively minimizing the least-squares difference of the experimental TWD and $|\psi_0(s)|^2$, where $\psi_0(s)$ is the numerical solution of Eq. (14) or its equivalent. In a test of this procedure, for very large or very small s the derived potential $\tilde{V}(s)$ was significantly different from the potential used to generate the “experimental” TWD, but they were quite close to each other over the range where the TWD is large, $0.5 \leq s \leq 1.5$. Hence, to improve estimates of the potential over a large range of ℓ , one should fit TWDs measured for several different misorientations (and, if possible, for different temperatures).

Applications to vicinal Cu surfaces is in progress [43]. Preliminary fits can account for secondary humps mentioned in Section 4 by invoking nonmonotonically decaying interactions and exponentially decaying tails.

5.3. Oscillatory interactions mediated by surface electronic states

The preceding subsection began with allusions to oscillatory electronic indirect interactions between steps [44]. When mediated by bulk electronic states, such interactions between atoms on surfaces decay rapidly with separation, but if mediated by surface states, the envelope of the oscillatory interaction has the same inverse-square behavior as the monotonic elastic, dipolar, and entropic repulsions:

$$\ell^{-2} \cos(2k_F\ell + \phi), \quad (15)$$

where k_F is the wave vector of the surface state at the Fermi level ⁴ and ϕ is a phase shift associated with scattering from the pair of steps.

Consistent behavior was seen in measurements of TWDs on vicinal Ag(110), including the

⁴ For non-circular states, the value of the wave vector in Eq. (15) is that along the Fermi “surface” at which the electron velocity is in the \hat{x} direction; see Ref. [44] for details.

presence of a surface state in the appropriate place in the surface Brillouin zone [45]. However, the evidence for the influence of surface states was not compelling due to the large number of fitting parameters compared to the amount of experimental data.

Convincing evidence of long-range, surface-state mediated interactions between Cu atoms on Cu{111} has just appeared [46]. It is tempting to invoke these interactions (which could even decay as $\ell^{-3/2}$ due to the isotropy of the state [47]) as the source of the large- s humps in “poor” data on this surface. However, this idea does not explain similar “poor” data on Cu{100}, where the image states are far from the Fermi energy.

The energy of the long-range interaction measured for Cu atoms on Cu{111} is notably weak [46]: the deepest minimum corresponds to an attraction of 0.4 meV at 27 Å. However, the consequent prefactor of the expression in Eq. (15) is 0.3 eV Å², which is comparable to the values of A listed in Table 2 (if some length of order an atomic spacing is used to adjust the units).

The transport properties of fractional metal overlayers have received close scrutiny in recent years [48]. Since the metallic surface states can be tuned in these systems, it is intriguing to speculate about engineering morphology using such step interactions.

6. Concluding remarks

The CGWD of Eq. (2) is an excellent interpolation between the established points at $\tilde{A} = 0$ and $\tilde{A} = 2$, and approaches the correct limit for very large \tilde{A} . Qualitatively it certainly captures the global behavior of variance as a function of \tilde{A} , and numerical evidence suggests that it interpolates well in the regime of large \tilde{A} . While the shape of the TWD does approach a Gaussian in this regime of moderately strong \tilde{A} , the CGWD (via Eq. (9)) provides arguably the best way to extract \tilde{A} from the variance of the TWD. Of the several ways to extract \tilde{A} from fits to a Gaussian, the Saclay (R) scheme is better for moderate \tilde{A} while the Grenoble (EA(all)) scheme is better for stronger \tilde{A} .

The difficulty of estimating accurately the value \tilde{A} from the TWD, especially from its variance or width, is exacerbated by the extreme sensitivity of σ^2 to \tilde{A} : fractional errors in the deduced widths of TWDs are magnified by a factor of 4 in \tilde{A} . For many applications, the relative size of the step-step repulsions between different systems is more important than their absolute sizes; thus, it is crucial that the analysis of \tilde{A} be done using the same approach. (Likewise, experimentalists should state clearly the raw (dimensionless) width, σ – or the value of ϱ in a fit to the CGWD.)

Often the extracted value is rationalized by misapplying the celebrated result of Marchenko and Parshin [49] relating the step repulsions to surface stress [49]. That formula assumes an elastically isotropic substrate and asymptotically large separations. Usually one, often both, of these conditions do not apply, and there is no well-prescribed procedure to compute corrections. Furthermore, the in-plane component of the stress dipole is not measurable and is often neglected. Thus, establishing quantitative connections between deduced \tilde{A} and surface stresses is (even) harder than extracting reliable quantitative estimates of \tilde{A} .

Another worrisome assumption is that the step interactions are “instantaneous” in the 1 + 1-D perspective (i.e. occur only between points on steps at the same coordinate along the mean step direction \hat{y}) becomes particularly questionable when steps are close together and have large wandering fluctuations with short wavelengths. In the latter situation, the description of single-step fluctuations in terms of stiffness may also break down.

In systems in which surface states near the Fermi energy play an active role, there should be notable effects on the TWD and the consequent surface morphology. Multistep correlations have received little attention, even though data is readily available in experiments measuring TWDs. Moreover, it is almost as easy to tabulate the step-step pair correlation function as the TWD, but easier to decipher theoretically. We have provided several hints and warnings, hopefully useful, for experimentalists studying spacings on vicinals.

Most theoretical activity dealing with random fluctuations in complex systems has focused on the the three special values of ϱ , and occasionally on

interpolations between them. This corresponds to weak \tilde{A} . The few exceptions focus on pair correlations and are rather technical [12]. More explicit numerical investigations in this regime would be illuminating. Moreover, there remains the mystery of why the CGWD works so well when there is no fundamental symmetry argument to justify it.

The Calogero–Sutherland model has been termed an ideal [14] Luttinger liquid [50,51]. Connections have been made to edge states in the quantum Hall effect [52], non-linear waves in a stratified fluid [53], and a host of more abstract problems. Most of these systems exhibit corrections, making it difficult to make detailed connections with the theory [14]. It will be interesting to see whether similar problems involving corrections to the A/ℓ^2 much discussed above confound a similar effort for vicinal surfaces. Furthermore, many of the interesting properties involve dynamic correlations, which for vicinal surfaces translates to correlations between displacements on (different) steps at *different* values of y . In any case, however, these connections between the properties of vicinal surfaces and other active fields add to the fascination of the subject.

Note added in proof, re Fig. 2

The Metropolis estimates of σ^2 in this preliminary figure are somewhat too small due to excessive weighting of data near the initial sharp distribution before equilibration. The correct values, depicted and discussed in Ref. [7], are in much better agreement with the n -fold way estimates and the CGWD curve.

Acknowledgements

Work was supported by the NSF-MRSEC at University of Maryland, done in collaboration with N. C. Bartelt, B. Joós, E. D. Williams, J. E. Reutt-Robey, et al. at UM, and with M. Giesen and H. Ibach at FZ-Jülich (via a Humboldt US Senior Scientist Award). SDC participated in an NSF-MRSEC-sponsored REU program. TLE's

work was also partially supported by NSF Grant EEC-0085604.

References

- [1] E.E. Gruber, W.W. Mullins, *J. Phys. Chem. Solids* 28 (1967) 875.
- [2] N.C. Bartelt, T.L. Einstein, E.D. Williams, *Surf. Sci.* 240 (1990) L591.
- [3] T.L. Einstein, O. Pierre-Louis, *Surf. Sci.* 424 (1999) L299.
- [4] M. Giesen, T.L. Einstein, *Surf. Sci.* 449 (2000) 191.
- [5] H.L. Richards, S.D. Cohen, T.L. Einstein, M. Giesen, *Surf. Sci.* 453 (2000) 59.
- [6] H.L. Richards, T.L. Einstein, *Phys. Rev. E*, submitted for publication, cond-mat/0008089 v2.
- [7] S.D. Cohen, H.L. Richards, T.L. Einstein, in preparation.
- [8] H.-C. Jeong, E.D. Williams, *Surf. Sci. Rep.* 34 (1999) 171.
- [9] S. van Dijken, H.J.W. Zandvliet, B. Poelsema, *Phys. Rev. B* 55 (1997) 7864.
- [10] M.L. Mehta, *Random Matrices*, second ed., Academic, New York, 1991.
- [11] T. Guhr, A. Müller-Groeling, H.A. Weidenmüller, *Phys. Rep.* 299 (1998) 189.
- [12] P.J. Forrester, *J. Stat. Phys.* 72 (1993) 39.
- [13] P.J. Forrester, private communication.
- [14] D. Sen, R.K. Bhaduri, *Can. J. Phys.* 77 (1999) 327.
- [15] O. Pierre-Louis, C. Misbah, *Phys. Rev. B* 58 (1998) 2265.
- [16] T. Ihle, C. Misbah, O. Pierre-Louis, *Phys. Rev. B* 58 (1998) 2289.
- [17] L. Masson, L. Barbier, J. Cousty, B. Salanon, *Surf. Sci.* 317 (1994) L1115.
- [18] C. Jayaprakash, C. Rottman, W.F. Saam, *Phys. Rev. B* 30 (1984) 6549.
- [19] V.Ya. Krivnov, A.A. Ovchinnikov, *Sov. Phys. JETP* 55 (1982) 162.
- [20] P.J. Forrester, *Nucl. Phys. B* 388 (1992) 671.
- [21] L. Barbier, L. Masson, J. Cousty, B. Salanon, *Surf. Sci.* 345 (1996) 197.
- [22] E. Le Goff, L. Barbier, L. Masson, B. Salanon, *Surf. Sci.* 432 (1999) 139.
- [23] F. Calogero, *J. Math. Phys.* 10 (1969) 2191.
- [24] F. Calogero, *J. Math. Phys.* 10 (1969) 2197.
- [25] B. Sutherland, *J. Math. Phys.* 12 (1971) 246.
- [26] B. Sutherland, *J. Math. Phys.* 12 (1971) 251.
- [27] F. Haake, *Quantum Signatures of Chaos*, Springer, Berlin, 1991.
- [28] A. Emundts, H.P. Bonzel, P. Wynblatt, K. Thürmer, J. Reutt-Robey, E.D. Williams, *Surf. Sci.* 481 (2001) 13.
- [29] Z.N.C. Ha, *Nucl. Phys. B* 435 (1995) 604.
- [30] F. Lesage, V. Pasquier, D. Serban, *Nucl. Phys. B* 435 (1995) 585.
- [31] F.D.M. Haldane, in: A. Okiji, N. Kawakami (Eds.), *Correlation Effects in Low-Dimensional Electronic Systems*, Springer, Berlin, 1994, p. 3.

- [32] N.C. Bartelt, T.L. Einstein, E.D. Williams, Surf. Sci. 276 (1992) 308.
- [33] N. Metropolis, A.W. Rosenbluth, M.N. Rosenbluth, A.H. Teller, E. Teller, J. Chem. Phys. 21 (1953) 1087.
- [34] A.B. Bortz, M.H. Kalos, J.L. Lebowitz, J. Comp. Phys. 17 (1975) 10.
- [35] M.A. Novotny, Comput. Phys. 9 (1995) 46.
- [36] K. Swamy, E. Bertel, I. Vilfan, Surf. Sci. 425 (1999) L369.
- [37] V.B. Shenoy, S. Zhang, W.F. Saam, Phys. Rev. Lett. 81 (1998) 3475.
- [38] B. Joós, T.L. Einstein, N.C. Bartelt, Phys. Rev. B 43 (1991) 8153.
- [39] H. van Beijeren, private communication.
- [40] D.R. Eisner, T.L. Einstein, Surf. Sci. 286 (1993) L559.
- [41] G.E.P. Box, W.G. Hunter, J.S. Hunter, Statistics for Experimenters: An Introduction to Design, Data Analysis, and Model Building, Wiley, New York, 1978.
- [42] A.Y. Abul-Magd, M.H. Simbel, Phys. Rev. E 60 (1999) 5371.
- [43] H.L. Richards, T.L. Einstein, M. Giesen, R. van Gastel, unpublished.
- [44] T.L. Einstein, in: W.N. Unertl (Ed.), Physical Structure of Solid Surfaces, Elsevier, Amsterdam, Handbook of Surface Science, vol. 1, N.V. Richardson, S. Holloway (Eds.), 1996, p. 577.
- [45] W.W. Pai, J.S. Ozcomert, N.C. Bartelt, T.L. Einstein, J.E. Reutt-Robey, Surf. Sci. 307–309 (1994) 747.
- [46] J. Repp, F. Moresco, G. Meyer, K.-H. Rieder, P. Hylgaard, M. Persson, Phys. Rev. Lett. 85 (2000) 2981.
- [47] R.C. Redfield, A. Zangwill, Phys. Rev. B 46 (1992) 4289.
- [48] S. Hasegawa, X. Tong, S. Takeda, N. Sato, T. Nagao, Prog. Surf. Sci. 60 (1999) 89.
- [49] V.I. Marchenko, A.Ya. Parshin, Sov. Phys. JETP 52 (1980) 129.
- [50] H.J. Schulz, G. Cuniberti, P. Pieri, Field Theories for Low-Dimensional Condensed Matter Systems, in: G. Morandi, P. Sodano, A. Tagliacozzo, V. Tognetti (Eds.), Springer, Berlin, 2000, Lecture Notes of the Chia Laguna Summer School, 1997, cond-mat/9807366v2.
- [51] J. Voit, in: Proceedings of the International Winterschool on Electronic Properties of Novel Materials 2000, cond-mat/0005114.
- [52] N. Kawakami, Phys. Rev. Lett. 71 (1993) 275.
- [53] H.H. Chen, Y.C. Lee, N.R. Pereira, Phys. Fluids 22 (1979) 187.
- [54] M. Giesen, G. Schulze Icking-Konert, Surf. Rev. Lett. 6 (1999) 27.
- [55] J.M. Bermond, J.J. Métois, J.C. Heyraud, F. Floret, Surf. Sci. 416 (1998) 430.
- [56] M. Giesen, Surf. Sci. 370 (1997) 55.
- [57] E.D. Williams, R.J. Phaneuf, J. Wei, N.C. Bartelt, T.L. Einstein, Surf. Sci. 310 (1994) 451.
- [58] X.-S. Wang, E.D. Williams, Surf. Sci. 400 (1998) 220.
- [59] K. Fujita, Y. Kusumi, M. Ichikawa, Phys. Rev. B 58 (1998) 1126.
- [60] C. Schwennicke, X.-S. Wang, T.L. Einstein, E.D. Williams, Surf. Sci. 418 (1998) 22.
- [61] E. Hahn, H. Scief, V. Marsico, A. Fricke, K. Kern, Phys. Rev. Lett. 72 (1994) 3378.